This paper is published as part of a PCCP Themed Issue on:
Metal oxide nanostructures: synthesis, properties and applications

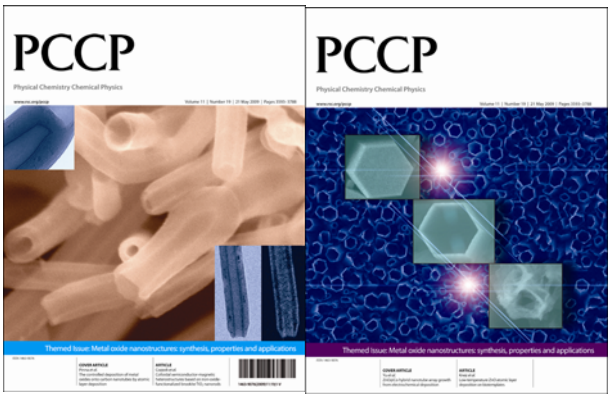

Guest Editors: Nicola Pinna, Markus Niederberger, John Martin Gregg and Jean-Francois Hochepied

Editorial

Chemistry and physics of metal oxide nanostructures
Phys. Chem. Chem. Phys., 2009
DOI: 10.1039/b905768d

Papers

Thermally stable ordered mesoporous CeO_2/TiO_2 visible-light photocatalysts
Guisheng Li, Dieqing Zhang and Jimmy C. Yu, *Phys. Chem. Chem. Phys.*, 2009
DOI: 10.1039/b819167k

Blue nano titania made in diffusion flames
Alexandra Teleki and Sotiris E. Pratsinis, *Phys. Chem. Chem. Phys.*, 2009
DOI: 10.1039/b821590a

Shape control of iron oxide nanoparticles
Alexey Shavel and Luis M. Liz-Marzán, *Phys. Chem. Chem. Phys.*, 2009
DOI: 10.1039/b822733k

Colloidal semiconductor/magnetic heterostructures based on iron-oxide-functionalized brookite TiO_2 nanorods
Raffaella Buonsanti, Etienne Snoeck, Cinzia Giannini, Fabia Gozzo, Mar Garcia-Hernandez, Miguel Angel Garcia, Roberto Cingolani and Pantaleo Davide Cozzoli, *Phys. Chem. Chem. Phys.*, 2009
DOI: 10.1039/b821964h

Low-temperature ZnO atomic layer deposition on biotemplates: flexible photocatalytic ZnO structures from eggshell membranes
Seung-Mo Lee, Gregor Grass, Gyeong-Man Kim, Christian Dresbach, Lianbing Zhang, Ulrich Gösele and Mato Knez, *Phys. Chem. Chem. Phys.*, 2009
DOI: 10.1039/b820436e

A LEEM/μ-LEED investigation of phase transformations in TiO_x/Pt(111) ultrathin films
Stefano Agnoli, T. Onur Menteş, Miguel A. Niño, Andrea Locatelli and Gaetano Granozzi, *Phys. Chem. Chem. Phys.*, 2009
DOI: 10.1039/b821339a

Synthesis and characterization of V_2O_3 nanorods
Alexander C. Santulli, Wenqian Xu, John B. Parise, Liusuo Wu, M.C. Aronson, Fen Zhang, Chang-Yong Nam, Charles T. Black, Amanda L. Tiano and Stanislaus S. Wong, *Phys. Chem. Chem. Phys.*, 2009
DOI: 10.1039/b822902c

Flame spray-pyrolyzed vanadium oxide nanoparticles for lithium battery cathodes
See-How Ng, Timothy J. Patey, Robert Büchel, Frank Krumeich, Jia-Zhao Wang, Hua-Kun Liu, Sotiris E. Pratsinis and Petr Novák, *Phys. Chem. Chem. Phys.*, 2009
DOI: 10.1039/b821389p

Mesoporous sandwiches: towards mesoporous multilayer films of crystalline metal oxides
Rainer Ostermann, Sébastien Sallard and Bernd M. Smarsly, *Phys. Chem. Chem. Phys.*, 2009
DOI: 10.1039/b820651c

Surprisingly high, bulk liquid-like mobility of silica-confined ionic liquids
Ronald Göbel, Peter Hesemann, Jens Weber, Eléonore Möller, Alwin Friedrich, Sabine Beuermann and Andreas Taubert, *Phys. Chem. Chem. Phys.*, 2009
DOI: 10.1039/b821833a

Fabrication of highly ordered, macroporous $Na_2W_4O_{13}$ arrays by spray pyrolysis using polystyrene colloidal crystals as templates
SunHyung Lee, Katsuya Teshima, Maki Fujisawa, Syuji Fujii, Morinobu Endo and Shuji Oishi, *Phys. Chem. Chem. Phys.*, 2009
DOI: 10.1039/b821209k

Nanoporous Ni–$Ce_{0.8}Gd_{0.2}O_{1.9-x}$ thin film cermet SOFC anodes prepared by pulsed laser deposition
Anna Infortuna, Ashley S. Harvey, Ulrich P. Muecke and Ludwig J. Gauckler, *Phys. Chem. Chem. Phys.*, 2009
DOI: 10.1039/b821473e

Surface chemistry of carbon-templated mesoporous aluminas
Thomas Onfroy, Wen-Cui Li, Ferdi Schüth and Helmut Knözinger, *Phys. Chem. Chem. Phys.*, 2009
DOI: 10.1039/b821505g

ZnO@Co hybrid nanotube arrays growth from electrochemical deposition: structural, optical, photocatalytic and magnetic properties
Li-Yuan Fan and Shu-Hong Yu, *Phys. Chem. Chem. Phys.*, 2009
DOI: 10.1039/b823379a

Electrochemistry of $LiMn_2O_4$ nanoparticles made by flame spray pyrolysis
T. J. Patey, R. Büchel, M. Nakayama and P. Novák, *Phys. Chem. Chem. Phys.*, 2009
DOI: 10.1039/b821572n

Ligand dynamics on the surface of zirconium oxo clusters
Philip Walther, Michael Puchberger, F. Rene Kogler, Karlheinz Schwarz and Ulrich Schubert, *Phys. Chem. Chem. Phys.*, 2009
DOI: 10.1039/b820731c

Thin-walled Er^{3+}:Y_2O_3 nanotubes showing up-converted fluorescence
Christoph Erk, Sofia Martin Caba, Holger Lange, Stefan Werner, Christian Thomsen, Martin Steinhart, Andreas Berger and Sabine Schlecht, *Phys. Chem. Chem. Phys.*, 2009
DOI: 10.1039/b821304f

Wettability conversion of colloidal TiO_2 nanocrystal thin films with UV-switchable hydrophilicity
Gianvito Caputo, Roberto Cingolani, Pantaleo Davide Cozzoli and Athanassia Athanassiou, *Phys. Chem. Chem. Phys.*, 2009
DOI: 10.1039/b823331d

Nucleation and growth of atomic layer deposition of HfO_2 gate dielectric layers on silicon oxide: a multiscale modelling investigation
A. Dkhissi, G. Mazaleyrat, A. Estève and M. Djafari Rouhani, *Phys. Chem. Chem. Phys.*, 2009
DOI: 10.1039/b821502b

Designing meso- and macropore architectures in hybrid organic–inorganic membranes by combining surfactant and breath figure templating (BFT)
Ozlem Sel, Christel Laberty-Robert, Thierry Azais and Clément Sanchez, *Phys. Chem. Chem. Phys.*, 2009
DOI: 10.1039/b821506e

The controlled deposition of metal oxides onto carbon nanotubes by atomic layer deposition: examples and a case study on the application of V_2O_4 coated nanotubes in gas sensing
Marc-Georg Willinger, Giovanni Neri, Anna Bonavita, Giuseppe Micali, Erwan Rauwel, Tobias Herntrich and Nicola Pinna, *Phys. Chem. Chem. Phys.*, 2009
DOI: 10.1039/b821555c

***In situ* investigation of molecular kinetics and particle formation of water-dispersible titania nanocrystals**
G. Garnweitner and C. Grote, *Phys. Chem. Chem. Phys.*, 2009
DOI: 10.1039/b821973g

Chemoresistive sensing of light alkanes with SnO_2 nanocrystals: a DFT-based insight
Mauro Epifani, J. Daniel Prades, Elisabetta Comini, Albert Cirera, Pietro Siciliano, Guido Faglia and Joan R. Morante, *Phys. Chem. Chem. Phys.*, 2009
DOI: 10.1039/b820665a

PCCP

Physical Chemistry Chemical Physics

www.rsc.org/pccp

Volume 11 | Number 19 | 21 May 2009 | Pages 3593–3788

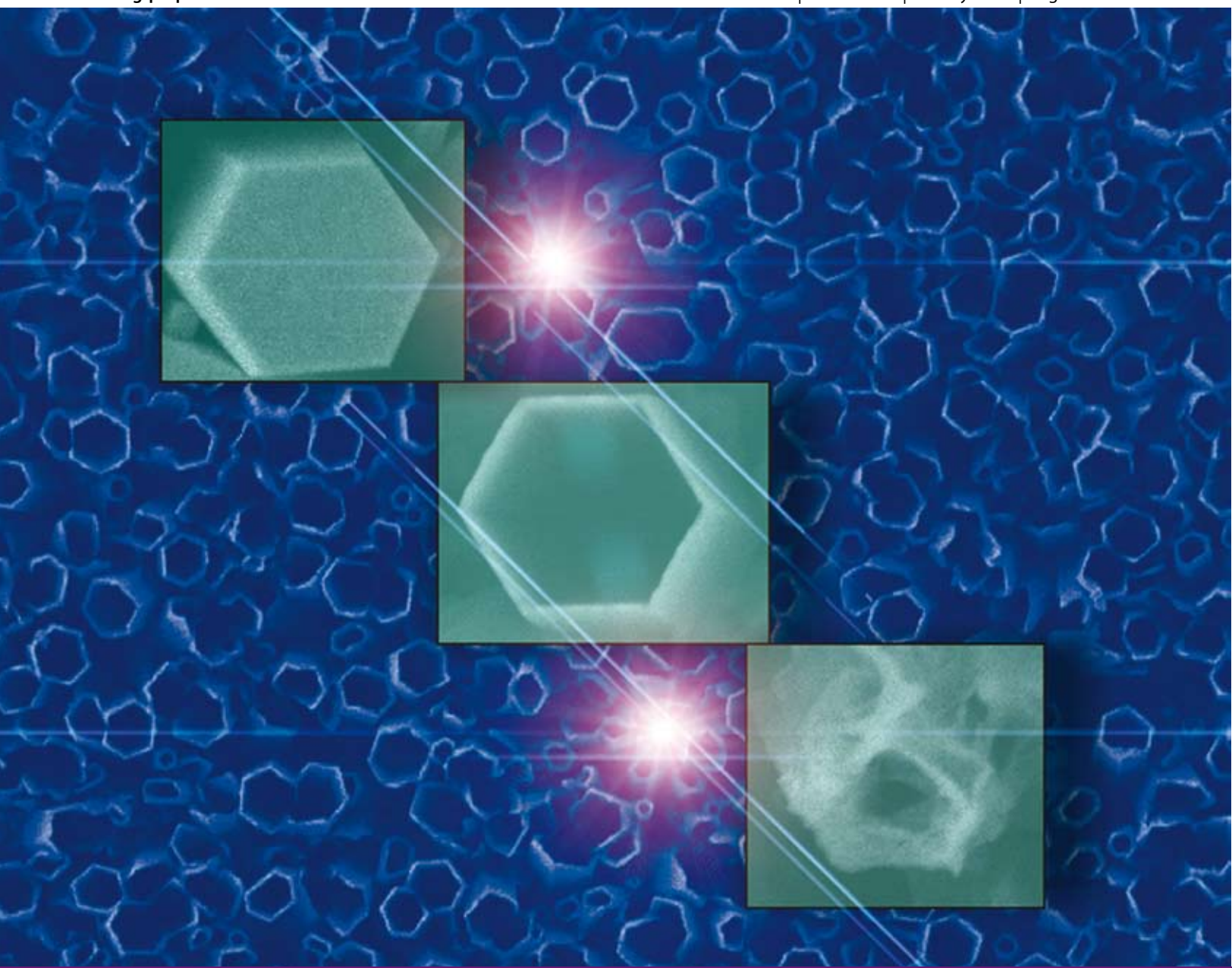

Themed Issue: Metal oxide nanostructures: synthesis, properties and applications

ISSN 1463-9076

ZnO@Co hybrid nanotube arrays growth from electrochemical deposition: structural, optical, photocatalytic and magnetic properties

Li-Yuan Fan and Shu-Hong Yu*

Received 7th January 2009, Accepted 24th February 2009
First published as an Advance Article on the web 24th March 2009
DOI: 10.1039/b823379a

Well-aligned ZnO@Co hybrid nanotube arrays on conductive glass substrates have been obtained by an electrochemical deposition approach. Vertical-aligned ZnO nanotubes with sizes between 300 and 600 nm in diameter and wall thickness of ~100 nm have been prepared by selective dissolution from the nanorods. The ZnO@Co heterostructures can be prepared by optimizing the deposition time and controlling the stability of Co^{2+} ions. Compared to the nanorod arrays, both nanotube arrays and the ZnO@Co heterostructures show enhanced photoluminescent properties. In addition, ZnO and ZnO@Co nanotubes show improved photocatalytic properties compared with the bare ZnO nanorod array, and the hybrid nanotubes exhibit better adsorptive properties than the bare ZnO nanotubes. Furthermore, the ZnO@Co hybrid nanotube arrays show ferromagnetism at room temperature.

1. Introduction

Semiconducting hybrid materials with improved functionalities such as optical, photocatalytic, electric and magnetic properties have attracted a lot of attention.[1–4] Especially, synthesis and properties of semiconductor–metal heterostructures such as ZnO–Au,[5,6] CdS–Au,[7] ZnO–Ag,[8] have been investigated in recent years due to their potential and important applications in catalysis, cellular imaging, immunoassay, luminescence tagging, and drug delivery. For example, if made magnetic, ZnO will become a kind of multifunctional material with semiconducting, optical, photocatalytic and magnetic properties.[9–12] Magnetic materials such as giant positive magnetic Co decorated nanomaterials would act as new members of the magnetic-semiconductor family.[13–15] Most hybrid materials are monolithic and not easy to be assembled into hybrid material devices.[1,2,4,9] Magnetic hybrid materials synthesized under mild conditions could offer obvious advantages in device design and fabrication.

ZnO, as a wide band-gap semiconductor (3.37 eV) with a large excitation binding energy (60 meV) at room temperature, has attracted much attention due to its remarkable near-UV emission, transparent conductivity, electric, and optical properties.[16] Recently, many well-defined ZnO nanostructures have been synthesized and widely studied.[17–25] Intensive research has been focused on constructing one-dimensional ZnO structures in large quantities.[20–25] In particular, hollow tubular structures exhibit a higher surface/volume ratio than bulk materials, and thus offer more chances for their applications in field-emission materials, gas sensors, photocatalysts, and nanoscale devices.[17,22,25] A typical ZnO nanotube array in large-scale has been synthesized by introducing a two-step electrochemical method.[25]

It is known that the choice of different growth method leads to a significant change in the quality of ZnO crystals.[24–27] Compared with physical methods, the chemical solution system is evidently low-temperature, low-cost and environmentally friendly. Recently, many ZnO nanostructures such as hexagonal ring-like superstructures, nanobrushes, patterned nanowires, nanorods, nanotubes, nanowires, nanosheets with porous morphology, heterostructures and some two-dimensional arrays, have been realized by an electrochemical method.[20,25,28–33] Choi *et al*. have fabricated lamellar, dendritic, mesoporous thin films, nanowires, three-dimensional porous films, cubic, octahedron, and other novel shapes of metal oxides *via* coupling of the electrochemical method and surfactant templating.[34–42] Parameters, such as temperature, ion concentration, potential, surfactant species, and electrodeposition time may tailor their morphology and affect their properties.[34] The morphology evolution can be tuned by kinetically controlling the growth rates of various facets through coupling the electrodeposition with capping agents.[28] Applying this new approach may develop a new system for investigating the process of crystal growth, which can stop and restart the reaction or change the reagents immediately without any delay.[34] What is more, it is possible to construct nanodevices on a large scale by utilizing this method, and to improve the performance of the nanomaterial.[25] Electrochemical synthesis strategy is a novel mild promising technique for fabrication of new heterostructures.

Herein, we report the synthesis of the heterostructure of ZnO@Co nanotube arrays by using the electrochemical deposition method. To the best of our knowledge, the nanotube arrays with magnetic mental wraps on the walls of each nanotube by electrodeposition have not been reported so far. The optical, magnetic, and photocatalytic properties of such heterostructures have been investigated.

Division of Nanomaterials and Chemistry, Hefei National Laboratory for Physical Sciences at Microscale, School of Chemistry and Materials, University of Science and Technology of China, Hefei, 230026, P. R. China. E-mail: shyu@ustc.edu.cn; Fax: +86 551 3603040

2. Experimental

2.1 Materials

$Zn(NO_3)_2{\cdot}6H_2O$, NH_4Ac, ethylenediamine (EDA), disodium ethylene diaminetetraacetate (EDTA) and $CoSO_4{\cdot}7H_2O$ were purchased from Sinopharm Chemical Reagent Co. Ltd. All reagents were of analytical grade and used without further purification. All glassware (glass bottle and small pieces of ITO (Indium Tin Oxides) glass substrates) was cleaned and sonicated in ethanol, rinsed with deionized (DI) water, and finally dried with acetone.

2.2 Preparation

The working electrode is an ITO glass substrate, with a sheet resistance of about 67 $\Omega\ cm^{-1}$ prepared by etching in a dilute HCl acid aqueous solution for a few seconds, then cleaned in deionized (DI) water three times. For the counter electrode, a Pt flag electrode is used. The reference electrode is a saturated calomel electrode (SCE), against which all the potential reported here was measured. Before electrodeposition, the three electrodes were all ultrasonically cleaned in DI water. The electrochemical experiments were conducted on a Multi-potentiostat (IM6ex, ZAHNER elektrik, Germany) using a conventional three-electrode system in an undivided cell.

2.3 Synthesis of ZnO nanotube arrays

Hexagonal ZnO rod arrays on the ITO substrates are electrodeposited at −1.20 V *versus* SCE for 10 h at 70 °C in the electrolyte of 0.05 M $Zn(NO_3)_2{\cdot}6H_2O$, 0.05 M NH_4Ac and 0.07 M EDA in an aqueous solution. Before routine electrodeposition, the seed-growth process is needed for the formation of regular *c*-axis preferential nanorod arrays. −1.40 V *versus* SCE for 300 s in the same solution at 70 °C is optimal for the seeding-growth process. After the routine electrodeposition, the nanorods covered with ITO substrate were rinsed in DI water several times and then acted as a working electrode during the second selective dissolution process. Typically, the etching solution consisted of 0.10 M EDA in DI water, and the temperature, time and applied potential were 70 °C, 3 h and −0.20 V *versus* SCE, respectively.

2.4 Synthesis of ZnO@Co nanotube array

After etching, the nanotubes covered ITO substrate was rinsed with DI water several times again, and then used as a working electrode for the third time. In a typical experiment, the third-step applied potential, deposition time and temperature were −1.80 V *versus* SCE, 10 min and 70 °C, respectively. The electrolyte is 0.05 M $CoSO_4{\cdot}7H_2O$ in aqueous solution here, and for the control experiment, 0.05 M $CoSO_4{\cdot}7H_2O$ with 0.5 M EDTA in aqueous solution was used.

2.5 Photocatalytic activity measurement

A cylindrical Pyrex flask (capacity *ca* 1000 mL) was used as the photoreactor vessel. The reaction system containing acid fuchsine ($C_{20}H_{17}N_3O_9S_3Na_2$) (Sigma-Aldrich Chemical Co.; 4.4×10^{-5} M, 100 mL) and ZnO or ZnO@Co nanotubes as catalyst (30 mg) was magnetically stirred in the dark for 5 min to reach the adsorption equilibrium of acid fuchsine with the catalyst, and then exposed to light from a Philips HPK high-pressure Hg lamp (125 W). Commercial TiO_2 (Degussa P25, Degussa Co.) was adopted as the reference with which to compare the photocatalytic activity under the same experimental conditions. UV-vis absorption spectra are recorded at different intervals to monitor the reaction. The acid fuchsine and photocatalytic agents used in the experiments were 100 ml (25 mg L^{-1}) and 30 mg, respectively.

2.6 Characterization

The final products were characterized by various techniques. X-Ray powder diffraction (XRD) was carried out on a Rigaku D/max-rA X-ray diffractometer with Cu Kα radiation (λ = 1.54178 Å). A scan rate of 0.05 s^{-1} was applied to record the pattern in the 2θ range of 10–90°. The morphology and size of the as-prepared products were observed by field emission scanning electron microscopy (FESEM), on a JSM-6700F field emission scanning electron microscope. High resolution TEM images (HRTEM) and the corresponding selected-area electron diffraction (SAED) patterns were recorded on a JEOL-2010 high-resolution transmission electron microscope at an acceleration voltage of 200 kV. To obtain further evidence for the purities and compositions of the as-prepared products, EDS (energy-dispersive X-ray spectroscopy) was conjunctionally used with HRTEM on Elementar Vario EL-III (Germany). Photoluminescence (PL) emission was performed at room temperature with a Perkin-Elmer LS55 luminescence spectrometer by radiation of 325 nm. UV-vis spectra are recorded on a Shimadzu UV-240 spectrophotometer at room temperature. The magnetism measurement was performed using a superconducting quantum interference device (SQUID) magnetometer (Quanyum Design, MPMS5XL). Room temperature electron paramagnetic resonance (EPR) was conducted on JEOL JES-FA200 EPR spectrometer (300 K, 9064 MHz, X-band).

3. Results and discussion

3.1 Seeds induced growth of ZnO arrays

The perpendicular ZnO nanorod array was constructed on the seeds buffer layer, which is a prerequisite for the subsequently regular growth. Fig. 1a shows that when no ZnO seed is prepared for the latter reaction, no regular serried ZnO nanorods are found, there are only a few random oriented hexagonal nanorods ranging from 300 to 600 nm in diameter and 4 μm in length seating on the substrate. The typical seeds buffer layer is obtained by a pre-electrodeposition in the same solution as the one used later at −1.40 eV for 300 s. Fig. 1b shows the seeds buffer layer with particle sizes ranging from 100 to 300 nm in diameter and the seeds are compactly arranged. In contrast, when the seeds buffer layer has been prepared for a subsequent synthesis, the same sized ZnO nanorods are aligned perpendicularly and at proportional spacing on the ITO conductive substrate, forming a two-dimensional array shown in Fig. 1c. The optimal seed-growth condition used in the present experiment is −1.40 V *versus* SCE for 300 s before regular electrodeposition. After seeds

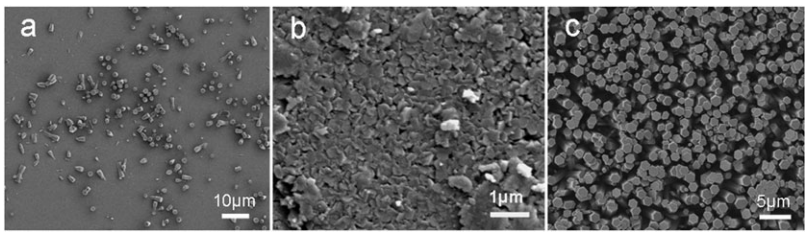

Fig. 1 Typical FE-SEM images of ZnO seeds buffer layer and nanorods grown without and with a seed buffer layer. (a) Random oriented nanorods, without a seeds buffer layer (−1.20 V *vs.* SCE for 6 h); (b) ZnO seeds buffer layer (−1.40 V *vs.* SCE for 300 s); (c) well-aligned nanorod array, with a seeds buffer layer (−1.40 V *vs.* SCE for 300 s and −1.20 V *vs.* SCE for 6 h). All experiments were conducted in aqueous solution at 70 °C.

growth, the latter deposition goes on immediately to construct a 1-D array.

3.2 Electrodeposition of ZnO@Co nanotube array

A homogeneous and well-aligned Co-coated ZnO nanotube array can be prepared through the electrodeposition of oriented ZnO nanorods, coordination-assisted selective dissolution and subsequently Co eletrodeposition in aqueous solution. Fig. 2a shows the XRD pattern of the heterostructure obtained by electrochemical growth in aqueous solution at 70 °C, which can be indexed as hexagonal ZnO and Co phases, respectively (Fig. 2b–c). The XRD patterns show that the as-synthesized Co coating ZnO nanotubes consist mainly of the *c*-axis orientated wurtzite ZnO. Some diffraction peaks in Fig. 2a can be indexed as pure hexagonal wurtzite ZnO with cell parameters $a = b = 1.63$ Å, $c = 2.61$ Å (JCPDS Card No. 5-664), and exhibits high crystallinity with a narrow diffraction peak. Some peaks can be indexed as a pure Co phase (JCPDS Card No. 5-727), and the diffraction peaks marked with asterisks are from the ITO substrate (JCPDS Card No. 6-395). A relatively higher intensity is observed for the 002 diffraction peak of the ZnO@Co nanotubes, indicating that the ZnO nanotubes could be well oriented, with the *c*-axis perpendicular to the substrate.

Fig. 3 shows typical FESEM images of a ZnO nanorod/nanotube array deposited in 0.05 M $Zn(NO_3)_2{\cdot}6H_2O$, 0.05 M NH_4Ac with 0.07 M EDA in aqueous solution. Previously, it was proposed that the preferential absorption of EDA on the (110) face of a hexagonal ZnO nanorod slows down the growth rate of the (110) face, and thus plays a major role for the formation of one dimensional nanorods during electrodeposition.[25] Large-scale and well-aligned dense nanorods stand on the substrate vertically (Fig. 3a). A high magnification image Fig. 3b shows that the rods with smooth surface are obviously hexagonal, and have mainly a diameter in the range of 300–600 nm. The ZnO nanotubes are formed through selective dissolution from the (001) surface straight into the bottom of the inner hole along the *c*-axis, as shown in Fig. 3c. A high resolution SEM image Fig. 3d shows that the ZnO nanotubes have a wall thickness of ~100 nm. The hexagonal facet shows that both the ZnO nanorods and nanotubes have a hexagonal wurtzite structure, as confirmed by the XRD results.

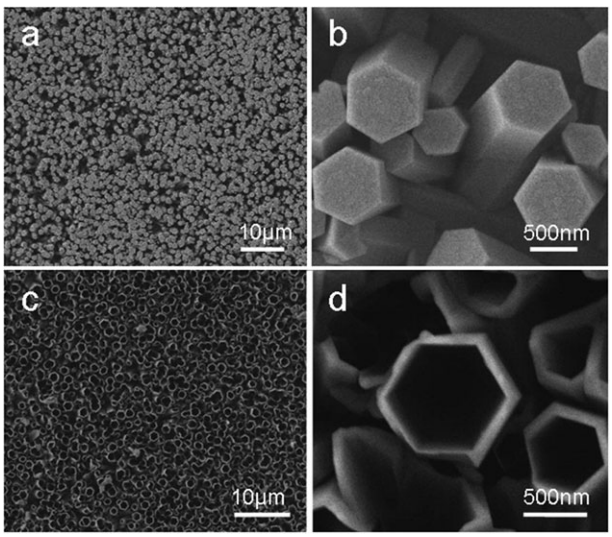

Fig. 3 FESEM images of (a), (b) the ZnO nanorod array grown by electrodeposition for 10 h in aqueous solution containing 0.05 M $Zn(NO_3)_2{\cdot}6H_2O$, 0.05 M NH_4Ac and 0.07 M EDA at 70 °C; and (c), (d) the ZnO nanotube array obtained by selective dissolution of the nanorod array shown in (a) , (b) in 0.10 M EDA for 3 h.

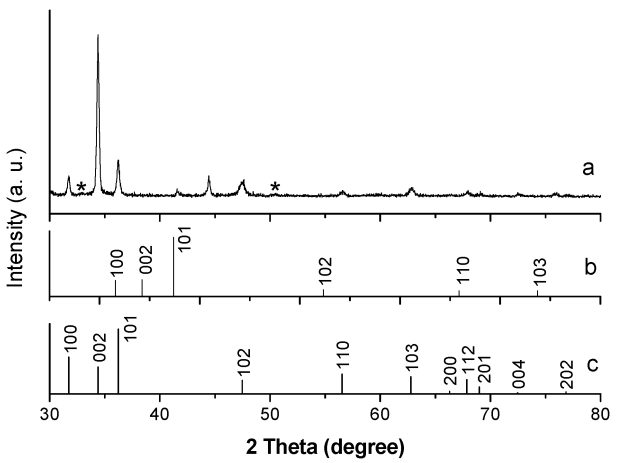

Fig. 2 XRD patterns of the product (a) obtained on the basal ZnO nanotube array in pure Co^{2+} ion solution at 70 °C for 10 min, and the standard XRD patterns of Co and ZnO (b), (c). The diffraction peaks of the substrate (SnO) are marked with an asterisk.

Fig. 4 shows the time dependent shape evolution process of the deposition of Co on ZnO nanotubes. Fig. 4a–c show leaf-like Co coatings covering the outer lateral surface of the nanotubes after deposition for 10 min, which are rather rougher compared to bare ZnO nanotubes. Leaf-like Co

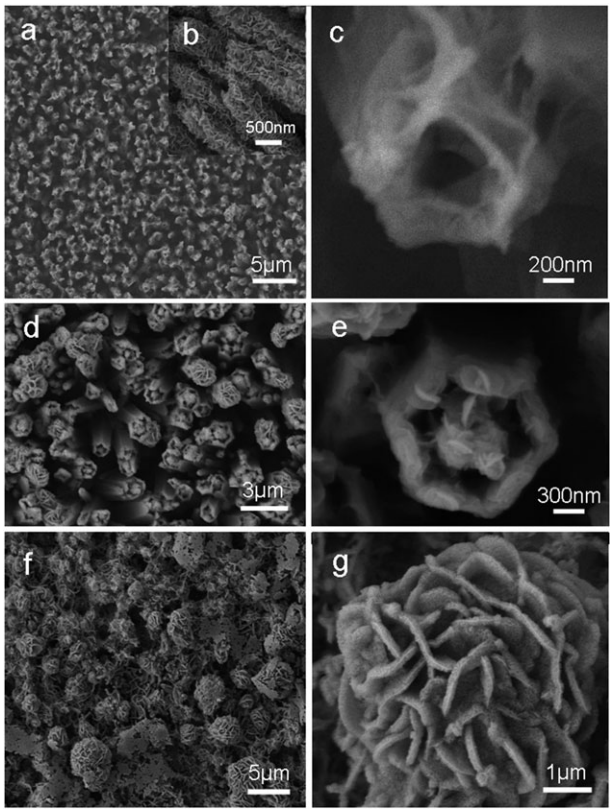

Fig. 4 FESEM images of the ZnO@Co nanotubes grown by electrodeposition of Co on the one-dimension ZnO nanotube array. The electrodeposition time is 10 min (a), (b), (c), 15 min (d), (e), and 20 min (f), (g). The electrodeposition is conducted in 0.05 M $CoSO_4 \cdot 7H_2O$ aqueous solution at 70 °C, −1.80 V *vs.* SCE.

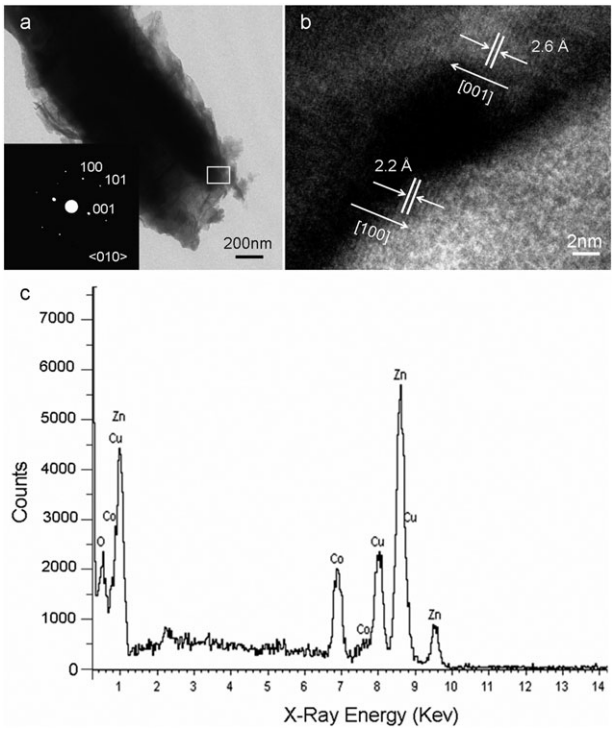

Fig. 5 (a) Low-magnification TEM image of an individual ZnO@Co heterostructure from the sample shown in Fig. 4a. (b) A HRTEM image of the ZnO@Co nanotube taken in the area marked by the rectangle. The insert is the corresponding SEAD pattern taken from the sample. (c) Energy-dispersive X-ray spectroscopy (EDS) taken from the selected area.

covers the outer walls almost uniformly through the whole nanotube, there is no obvious difference between the top and the bottom of a single nanotube (Fig. 4b). When the reaction time exceeds 10 min, cauliflower-like Co nanoballs will form and fill into the hollow part of the ZnO nanotubes. Fig. 4d shows the two-dimensional ZnO@Co nanotube array with a Co crest on almost each ZnO@Co nanotube, and there are even a few Co microballs at the top surface of the array. The ZnO@Co nanotube with a Co crest on it is shown in Fig. 4e, and the crest-like Co in the hole of the nanotube is ~300 nm in diameter, smaller than the Co microballs at the top surface of the array. The leaf-like Co particles congregate with each other to form cauliflower-like Co nanoballs/microballs without the support of the ZnO tubes. The cauliflower-like Co microballs with a diameter from 0.5 to 4 μm mantle on the array (Fig. 4f–g).

The structural details of the ZnO@Co heterostructures were further studied by high resolution TEM (HRTEM) and energy-dispersive X-ray spectroscopy (EDS). After being scraped from the substrate and ultrasonicated in ethanol, the original structure can still be observed. Fig. 5a shows the hollow structure of ZnO@Co with a diameter of ~500 nm and a wall thickness of ~100 nm, the leaf-like Co coats the outer surface of the ZnO nanotube. The HRTEM image in Fig. 5b demonstrates the single-crystal nature of the ZnO nanotube with the lattice interplanar spacing along the length direction of 2.6 Å, corresponding to the lattice spacing of the (002) plane of hexagonal wurtzite ZnO. The interplanar spacing of 2.6 Å observed in the outer layer corresponds to that of the (100) plane of the Co phase, which suggests epitaxial growth of the Co layers on the ZnO nanotubes. The insert in Fig. 5a shows that the electron diffraction (SAED) pattern of the selected area further indicates single crystallinity of the ZnO tube. No Co diffraction is observed, which may be ascribed to the tiny quantity of the Co element. The EDS analysis (Fig. 5c) proves that Co, Zn and O elements can be detected, the molar ratio of Co in ZnO@Co is 11.1%. The peaks of Cu come from the Cu grid used in the experiment.

3.3 Possible growth mechanism of ZnO@Co nanotube arrays

A possible growth mechanism of ZnO@Co nanotube arrays has been proposed. At the beginning of the Co coating process, Co^{2+} ions discharge on the negative-charge places of ZnO nanotubes, and first accrete on the (110) surface (shown in Fig. 4a–c). As the reaction continues, the leaf-like Co particles form and grow thicker and thicker. With depositing time prolonged, a similar morphology of the leaf-like Co on the lateral surfaces is also observed in the Co nanoballs/microballs, which suggests a similar growth mechanism of Co on either the lateral surfaces of the nanotubes or the top surface of the array. The default experiments confirmed that only cauliflower-like Co microballs formed if no ZnO nanotubes were grown on the ITO substrate.

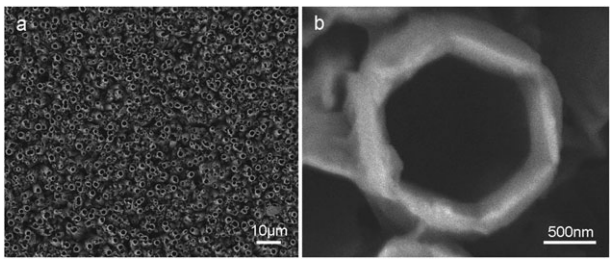

Fig. 6 Co electrodeposition on 1-D ZnO nanotube array. The reaction time and the applied potential are 10 min and −1.80 V *versus* SCE, respectively. The electrolyte used here is 0.05 M $CoSO_4{\cdot}7H_2O$ with 0.5 M EDTA in aqueous solution.

A slight change in the stability of Co^{2+} ions may affect the reaction rate and thus affect the morphology. A control experiment was performed, in which 0.5 M EDTA was added to the 0.05 M $CoSO_4{\cdot}7H_2O$ solution. Fig. 6 shows typical SEM micrographs, where smooth and compact Co plating on the lateral walls of ZnO nanotubes is observed. The differences between the two kinds of Co-coating (shown in Fig. 4a–c and Fig. 6, respectively) on nanotubes indicate that the states of Co^{2+} ions (or the concentration of $[Co^{2+}]_{free}$) have a significant influence on the morphology of Co coatings. The different reaction equations are listed in eqns (1)–(2) ($\varphi^{\theta} = -0.277$ V).

$$Co^{2+} + 2e \rightarrow Co,\ \varphi_1 = \varphi^{\theta} + \frac{0.059}{2}\lg[Co^{2+}]_{free1} \quad (1)$$

$$[Co(EDTA)]^{2-} + 2e \rightarrow Co,\ \varphi_1 = \varphi^{\theta} + \frac{0.059}{2}\lg[Co^{2+}]_{free2} \quad (2)$$

According to the electrochemical reactions in eqns (1–2), with adding EDTA to the Co^{2+} electrolyte, the Co^{2+} ions will complex with $EDTA^{4-}$ to form $[Co(EDTA)]^{2-}$, and the concentration of free Co^{2+} ions will decrease. Because $[Co^{2+}]_{free2} < [Co^{2+}]_{free1}$ and $\varphi_1 > \varphi_2$, it needs a more negative voltage to discharge, thus the reaction rate is slower at the same voltage when EDTA is added to the system. The Co layer deposited in the presence of EDTA is smoother than the one without EDTA, here the EDTA complexants capture free Co^{2+} ions to increase their stability, thereby it will slow down the reaction rate, which will favor the formation of a smoother and more compact Co layer. The influence of the complex agent on the morphology and properties needs a more detailed investigation in the future.

3.4 Optical and magnetic properties

The room temperature photoluminescence (PL) spectra of the samples with different structures prepared by electrodeposition were measured. All three samples exhibit strong band-edge emissions at *ca* 383 nm due to free-exciton recombination, and weak broad green emissions centered at *ca* 530 nm related to the defects in the ZnO such as annihilation of electrons with holes trapped in singly ionized oxygen vacancies.[20]

The UV region emission intensity of the well-aligned ZnO nanorods is less than that of the nanotubes (marked with a and b, respectively, in Fig. 7). In the present experiments, the same

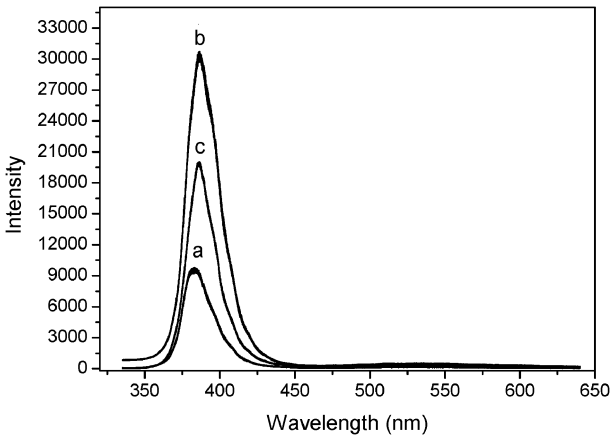

Fig. 7 Room temperature PL spectra of a well-aligned ZnO nanorod/nanotube array and a ZnO@Co nanotube array on ITO substrate. (a) ZnO nanorods, (b) ZnO nanotubes, (c) ZnO@Co nanotubes. The counterpart of ZnO in ZnO bare nanotubes and ZnO@Co hybrid nanotubes are both about 15 mg.

quality and less quantity of ZnO in nanotubes than in ZnO nanorods make it unlikely to arouse the enhancement of UV region emission. Thus, the UV region emission differences observed in Fig. 7 could be ascribed to the size effect of the nanostructures and the crystallinity. The higher surface/volume ratio of the ZnO nanotubes also results in enhancement of the UV emission. The selective dissolution process of nanorods to nanotubes is useful for improving the quality of the 1D nanomaterials and the dissolution process usually more easily starts at the places with more defects. The position of the UV emission peak exhibits a slight red-shift for ZnO nanotubes from ~383 to ~386 nm, corresponding to the structure differences between nanorods and nanotubes. The ZnO tubular structure with wall thickness smaller than the optical wavelength while larger than the exciton Bohr radius makes it possible for the spatial confinement in both two dimensions, and therefore increases the lifetime and bonding-energy of the exciton and brings about a lower threshold power for the emission.[25] For the differences between ZnO nanotubes and ZnO@Co heterostructures, the UV emission intensity only decreases to some extent which is due to the Co covered on the ZnO surface (Fig. 7b,c). Compared with the ZnO nanotube array, the ZnO@Co herterostructures did not show a shift in its PL spectrum, suggesting that the red-shift is mainly caused by the structure transformation from nanorods to nanotubes.

The magnetic properties of the ZnO@Co nanotube array have also been investigated. The most remarkable result shown in Fig. 8 is the ferromagnetism indicated by the well-defined magnetic hysteresis loop of 11.1% at Co coated ZnO nanotubes at room temperature. The punch-like M–H curve indicates the strong room-temperature ferromagnetism of the heterostructure. The coercivity (H_c) of the ZnO@Co heterostructure is about 150 Oe. The magnetic hysteresis loop consists in a previous report by Tian *et al.*[13]

To further demonstrate the ferromagnetic properties of the hybrid ZnO@Co nanotubes, an electron paramagnetic resonance measurement is performed. Fig. 9 demonstrates the

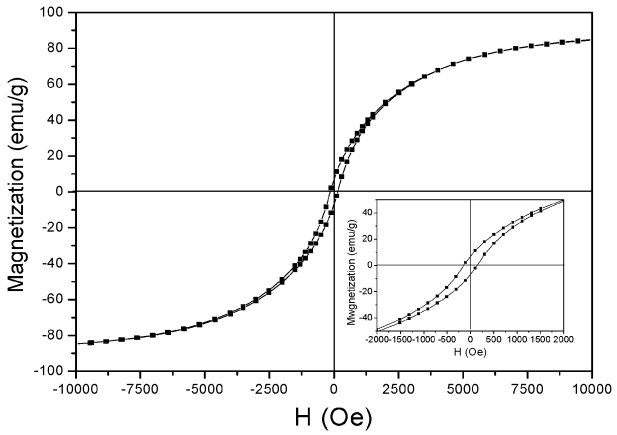

Fig. 8 Magnetic hysteresis loop of the Co-coating ZnO nanotube array after electrodeposition for 10 min at room temperature (300 K). Insert: enlarged plot of the *M–H* curve.

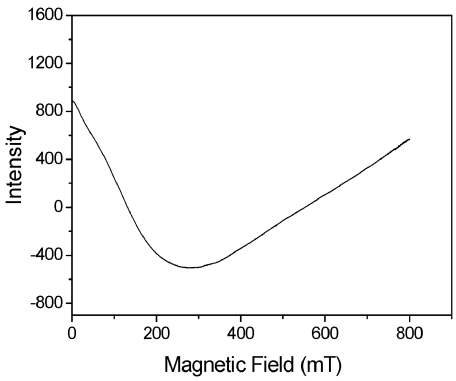

Fig. 9 The electron paramagnetic resonance (EPR) spectrum of the ZnO@Co nanotube array prepared after electrodeposition for 10 h, and selective dissolution for 3 h, and Co coating for 10 min at 70 °C in aqueous solution.

obvious ferromagnetic properties of ZnO@Co hybrid nanotubes, which can be estimated from the broad concave on the curve.[43] The hybrid particles scraped from ITO substrates can give a quick response to an external magnet at room temperature, as shown in Fig. 10.

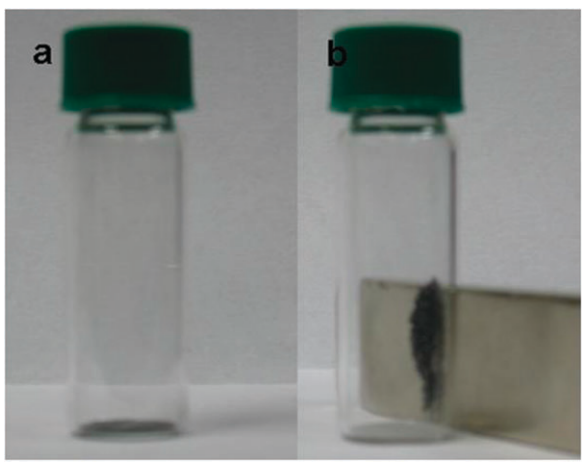

Fig. 10 The magnetic response of the magnet operation on the product.

3.5 Photocatalytic activity properties

It is well-known that ZnO has been used as a semiconductor-type photocatalyst for the photocatalytic degradation of water pollutants, photoreductive dehalogenation of halogenated benzene derivatives, and photocatalytic reduction of toxic metal ions.[44] Recently, 1-D ZnO nanostructured arrays, such as nanobelts and nanowires have been tested as immobilized photocatalysts due to their expected high photocatalytic activity attributed to the high surface-to-volume ratio, and recyclable characteristics.[45] To demonstrate the potential applicability of the as-synthesized ZnO and ZnO@Co nanotubes in these applications, their photocatalytic activity was examined by choosing photocatalytic degradation of acid fuchsine as a test reaction. Time-dependent UV-vis absorption spectra of photocatalysis degraded acid fuchsine were recorded (Fig. 11a–b). The characteristic absorption of acid fuchsine at about 543 nm was chosen as the monitored

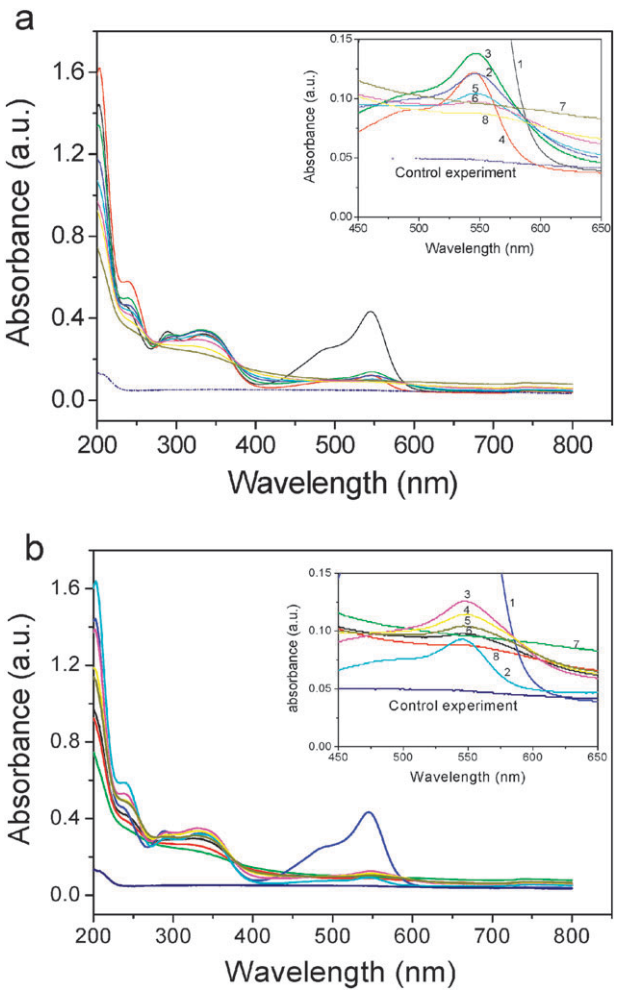

Fig. 11 Time-dependent absorption spectra of a solution of acid fuchsine (4.4×10^{-5} M, 100 mL) in the presence of (a) ZnO nanotubes (30 mg) and (b) ZnO@Co nanotubes (30 mg) prepared by electrodeposition for 10 h, dissolution for 3 h, and Co deposition for 10 min. Note: (1) initial solution; (2) after adding the ZnO and ZnO@Co nanotubes; and (3)–(8) after exposure to UV light for (3) 5, (4) 15, (5) 25, (6) 35, (7) 45, (8) 60 min. The controlled experiment was carried out in the presence of 30 mg TiO_2 after exposure for 60 min.

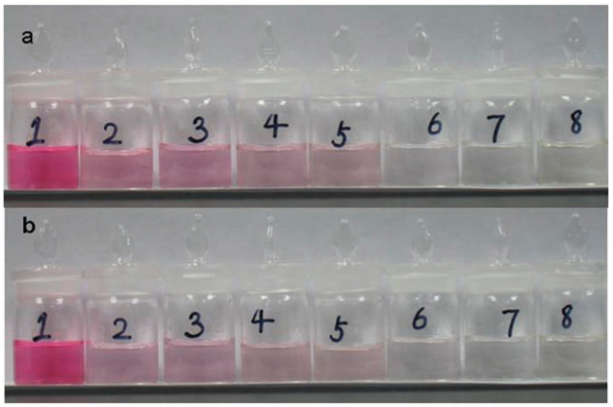

Fig. 12 Time-dependent color change of the samples. Time-dependent colour change of a solution of acid fuchsine (4.4×10^{-5} M, 100 mL) in the presence of (a) ZnO nanotubes (30 mg) and (b) ZnO@Co nanotubes (30 mg) prepared by electrodeposition for 10 h, dissolution for 3 h, and Co deposition for 10 min. Note: (1) initial solution; (2) after adding the ZnO and ZnO@Co nanotubes; and (3)–(8) after exposure to UV light for (3) 5, (4) 15, (5) 25, (6) 35, (7) 45, (8) 60 min.

parameter for the photocatalytic degradation process. Commercial TiO_2 was adopted as the reference with which to compare the photocatalytic activity under the same experimental conditions. Both the ZnO and ZnO@Co nanotubes were scraped from ITO substrates and were then uniformly dispersed in the acid fuchsine solution for the test. A series of color changes corresponding to the sequential changes detected by the UV-vis absorption spectra are shown in Fig. 12. As shown in Fig. 11, the absorbance intensity for the peak at 543 nm decreases remarkably once the ZnO or ZnO@Co nanotubes are added, corresponding to the immediate color change shown in Fig. 12. The results suggest that the ZnO and ZnO@Co nanotubes may have a high surface/volume ratio and can thus adsorb the dye molecules efficiently. The acid fuchsine with ZnO@Co hybrid nanotubes display a more evident color change, which suggests that the hybrid structure possesses a higher surface/volume ratio and has more absorptive ability, and the higher surface/volume ratio may be induced by the leaf-like Co coating on the ZnO nanotubes. With exposure time prolonging, the typical sharp peak at 543 nm diminishes gradually and vanishes completely after 45 min. In comparison with the commercial TiO_2 (dot line), the ZnO and ZnO@ Co nanotubes did not show a prominent photocatalytic activity (inserts in Fig. 11). The colour diminishing rate in the presence of ZnO@Co nanotubes is faster than that in the presence of bare ZnO nanotubes (Fig. 12). The present results demonstrated that the ZnO@Co hybrid structure shows some improvement on its photocatalytic activity properties.

4. Conclusions

In summary, well-aligned ZnO@Co hybrid nanotube arrays with diameters ranging from 300 to 600 nm and a length of $\sim$5 μm on conductive glass substrates have been synthesized *via* an electrochemical deposition approach. The key factor for the preparation of a vertically oriented ZnO nanorod/nanotube array is to prepare a well-oriented seeds buffer layer at first. The formation of leaf-like Co on ZnO nanotubes is strongly dependent on the reaction time and the states of the Co^{2+} ions/the concentration of $[Co^{2+}]_{free}$ in the solution. Three different structures exhibit a different optical performance, which may be due to the different structural features (surface/volume ratio) and the crystallinity. Both ZnO and ZnO@Co nanotubes show good photocatalytic and absorptive properties. The ZnO@Co hybrid nanotube arrays exhibit room temperature ferromagnetic properties. The present synthesis method by combination with the selective dissolution and later on electrochemical deposition may make it possible to access a variety of hybrid nanostructured materials in other systems.

This work is supported by the National Science Foundation of China (NSFC) (Grants Nos. 50732006, 20621061, 20671085), 2005CB623601 and the Partner-Group of the Chinese Academy of Sciences-the Max Planck Society.

References

1 S. Mathews, R. Ramesh, T. Venkatesan and J. Benedetto, *Science*, 1997, **276**, 238.
2 G. Y. Shan, M. Y. Zhong, S. Wang, Y. J. Li and Y. C. Liu, *J. Colloid Interface Sci.*, 2008, **326**, 392.
3 K. Griffin Roberts, M. Varela, S. Rashkeev, S. T. Pantelides, S. J. Pennycook and K. M. Krishnan1, *Phys. Rev. B*, 2008, **78**, 014409.
4 M. Zanella, A. Falqui, S. Kudera, L. Manna, M. F. Casula and W. J. Parak, *J. Mater. Chem.*, 2008, **18**, 4311.
5 W. Q. Zhang, Y. Lu, T. K. Zhang, W. P. Xu, M. Zhang and S. H. Yu, *J. Phys. Chem. C*, 2008, **112**, 19872.
6 X. Wang, X. G. Kong, Y. Yu and H. Zhang, *J. Phys. Chem. C*, 2007, **111**, 3836.
7 A. E. Saunders, I. Popov and U. Banin, *J. Phys. Chem. B*, 2006, **110**, 25421.
8 C. Pacholski, A. Kornowski and H. Weller, *Angew. Chem.*, 2004, **116**, 4878.
9 G. H. Ji, Z. B. Gu, M. H. Lu, D. Wu, S. T. Zhang, Y. Y. Zhu, S. N. Zhu and Y. F. Chen, *J. Phys.: Condens. Matter*, 2008, **20**, 425207.
10 Q. Y. Xu, L. Hartmann, S. Q. Zhou, A. Mcklich, M. Helm, G. Biehne, H. Hochmuth, M. Lorenz, M. Grundmann and H. Schmidt, *Phys. Rev. Lett.*, 2008, **101**, 076601.
11 N. Sanchez, S. Gallego and M. C. Muñoz, *Phys. Rev. Lett.*, 2008, **101**, 067206.
12 T. F. Jaramillo, S. H. Baeck, A. Kleiman-Shwarsctein, K. S. Choi, G. D. Stucky and E. W. McFarland, *J. Combinat. Chem.*, 2005, **7**, 264.
13 Y. F. Tian, J. Antony, R. Souza, S. S. Yan, L. M. Mei and Y. Qiang, *Appl. Phys. Lett.*, 2008, **92**, 192109.
14 C. D. Pemmaraju, R. Hanafin, T. Archer, H. B. Braun and S. Sanvito, *Phys. Rev. B*, 2008, **78**, 054428.
15 Y. Fukuma, *Phys. Rev. B*, 2008, **78**, 104417.
16 Ü. Özgür, Y. I. Alivov, C. Liu, A. Teke, M. A. Reshchikov, S. Dogan, V. Avrutin, S. J. Cho and H. Morkoçd, *J. Appl. Phys.*, 2005, **98**, 041301.
17 Y. J. Xing, Z. H. Xi, Z. Q. Xue, X. D. Zhang and J. H. Song, *Appl. Phys. Lett.*, 2003, **83**, 1689.
18 A. B. Djurisic, W. M. Kwok, Y. H. Leung, D. L. Phillips and W. K. Chan, *J. Phys. Chem. B*, 2005, **109**, 19228.
19 J. B. Liang, J. W. Liu, Q. Xie, S. Bai, W. C. Yu and Y. T. Qian, *J. Phys. Chem. B*, 2005, **109**, 9463.
20 J. B. Cui, *J. Phys. Chem. C*, 2008, **112**, 10385.
21 D. Tainoff, B. Masenelli, O. Boisron, G. Guiraud and P. Melinon, *J. Phys. Chem. C*, 2008, **112**, 12623.
22 Y. H. Tong, Y. C. Liu, C. L. Shao, Y. X. Liu, C. S. Xu, J. Y. Zhang, Y. M. Lu, D. Z. Shen and X. W. Fan, *J. Phys. Chem. B*, 2006, **110**, 14714.
23 W. I. Park, D. H. Kim, S. W. Jung and G. C. Yi, *Appl. Phys. Lett.*, 2003, **83**, 964.

24 X. D. Yan, Z. W. Li, R. Q. Chen and W. Gao, *Cryst. Growth Des.*, 2008, **8**, 2406.
25 L. F. Xu, Q. Liao, J. P. Zhang, X. C. Ai and D. S. Xu, *J. Phys. Chem. C*, 2007, **111**, 4549.
26 X. D. Wang, Y. Ding, C. J. Summers and Z. L. Wang, *J. Phys. Chem. B*, 2004, **108**, 8773.
27 Y. Zhang, H. B. Jia, X. H. Luo, X. H. Chen, D. P. Yu and R. M. Wang, *J. Phys. Chem. B*, 2003, **107**, 8289.
28 Z. L. Xiao, C. Y. Han, W. K. Kwok, H. H. Wang, U. Welp, J. Wang and G. W. Crabtree, *J. Am. Chem. Soc.*, 2004, **126**, 2316.
29 S. Xu, Y. G. Wei, M. Kirkham, J. Liu, W. J. Mai, G. Davidovic, R. L. Snyder and Z. L. Wang, *J. Am. Chem. Soc.*, 2008, **130**, 14958.
30 H. D. Yu, Z. P. Zhang, M. Y. Han, X. T. Hao and F. R. Zhu, *J. Am. Chem. Soc.*, 2005, **127**, 2378.
31 M. Fu, J. Zhou, Q. F. Xiao, B. Li, R. L. Zong, W. Chen and J. Zhang, *Adv. Mater.*, 2006, **18**, 1001.
32 L. F. Xu, Y. Guo, Q. Liao, J. P. Zhang and D. S. Xu, *J. Phys. Chem. B*, 2005, **109**, 13519.
33 C. Mu, Y. X. Yu, R. M. Wang, K. Wu, D. S. Xu and G. L. Guo, *Adv. Mater.*, 2004, **16**, 17.
34 K. S. Choi, *Dalton Trans.*, 2008, 5423.
35 E. M. P. Steinmiller and K. S. Choi, *Langmuir*, 2007, **23**, 12710.
36 Y. W. Tan, E. M. P. Steinmiller and K. S. Choi, *Langmuir*, 2005, **21**, 9618.
37 C. M. Lopez and K. S. Choi, *Langmuir*, 2006, **22**, 10625.
38 S. H. Baeck, K. S. Choi, T. F. Jaramillo, G. D. Stucky and E. W. McFarland, *Adv. Mater.*, 2003, **15**, 15.
39 Y. W. Tan, S. Srinivasan and K. S. Choi, *J. Am. Chem. Soc.*, 2005, **127**, 3596.
40 K. S. Choi, H. C. Lichtenegger and G. D. Stucky, *J. Am. Chem. Soc.*, 2002, **124**, 12402.
41 C. Santato, C. M. Lopez and K. S. Choi, *Electrochem. Commun.*, 2007, **9**, 1519.
42 R. L. Spray and K. S. Choi, *Chem. Commun.*, 2007, 3655.
43 R. Boubekri, Z. Beji, K. Elkabous, F. Herbst, G. Viau, S. Ammar, F. Fiévet, H. J. von Bardeleben and A. Mauger, *Chem. Mater.*, 2009, DOI: 10.1021/cm802605u.
44 W. T. Yao, S. H. Yu, S. J. Liu, J. P. Chen, X. M. Liu and F. Q. Li, *J. Phys. Chem. B*, 2006, **110**, 11704.
45 Y. J. Tak, H. Y. Kim, D. W. Lee and K. J. Yong, *Chem. Commun.*, 2008, 4585.